The Astrophysical Journal, 953:63 (12pp), 2023 August 10 https://doi.org/10.3847/1538-4357/acdd6e

Orbital Period Variations in HT Cas: Evidence for Additional Angular Momentum Loss and a High-eccentricity Giant Planet

Z.-T Han[1,2,3,4], S.-B Qian[2,3,4,5,6], Q.-W Han[7], L. Zang[2,3,5], B. Soonthornthum[8], L.-J Li[2,3,4], L.-Y. Zhu[2,3,4,5], W. Liu[2,3,5], E. Fernández Lajús[9,10], Z.-B Dai[2,3,4], and W.-W Na[1]

[1] Department of Physics, Yuxi Normal University, Phoenix Road 134, 653100 Yuxi, People's Republic of China; hzt@yxnu.edu.cn
[2] Yunnan Observatories, Chinese Academy of Sciences (CAS), P.O. Box 110, 650216 Kunming, People's Republic of China
[3] Key Laboratory of the Structure and Evolution of Celestial Objects, Chinese Academy of Sciences, P.O. Box 110, 650216 Kunming, People's Republic of China
[4] Center for Astronomical Mega-Science, Chinese Academy of Sciences, 20A Datun Road, Chaoyang District, Beijing, 100012, People's Republic of China
[5] University of Chinese Academy of Sciences, Yuquan Road 19#, Sijingshang Block, 100049 Beijing, People's Republic of China
[6] Guizhou Provincial Key Laboratory of Radio Data Processing, School of Physics and Electronic Sciences, Guizhou Education University, Guiyang 550001, People's Republic of China
[7] School of Physics and Electronics, Qiannan Normal University for Nationalities, Duyun 558000, People's Republic of China
[8] National Astronomical Research Institute of Thailand, Ministry of Higher Education Science Research and Innovation, 260 Moo 4, T. Donkaew, A. Maerim, Chiangmai, 50180, Thailand
[9] Facultad de Ciencias Astronómicas y Geofísicas, Universidad Nacional de La Plata, Paseo del Bosque s/n, 1900 La Plata, Buenos Aires, Argentina
[10] Instituto de Astrofísica de La Plata (CCT La Plata CONICET/UNLP), 1900 La Plata, Argentina
Received 2022 June 26; revised 2023 May 14; accepted 2023 May 19; published 2023 August 2

Abstract

We present a timing study of the short-period eclipsing cataclysmic variable (CV) HT Cas. Based on new eclipse times derived from our photometric monitoring and archival optical data, combined with historical timings, spanning ∼42 yr, we detect a secular decrease in the orbital period at a rate of $\dot{P} = -1.32 \times 10^{-12}$ ss^{-1} and a cyclic period wiggle with an amplitude of 79.3 s and a period of 30.28 yr. We find that neither gravitational radiation nor magnetic braking can explain the observed decrease rate, suggesting the presence of additional angular momentum loss (AML). The empirical consequential AML (eCAML) model developed by Schreiber et al. can well match the observed orbital decay in HT Cas, and the physical mechanism for eCAML is most likely attributable to the frictional AML following nova eruptions. As for the cyclic variation, the best explanation is the influence of an unseen companion in orbit around the binary. The derived orbital parameters reveal that the hypothetical third body could be a giant planet with mass of $M_3 \simeq 14 M_{\rm Jup}$ that is moving on a highly eccentric orbit ($e = 0.82$). Taken together the results of the present study suggest that HT Cas is a unique triple system containing a high-eccentricity giant planet and it has the potential to become an ideal laboratory in which to test models of CV evolution.

Unified Astronomy Thesaurus concepts: Close binary stars (254); Eclipsing binary stars (444); Cataclysmic variable stars (203); Dwarf novae (418)

Supporting material: machine-readable table

1. Introduction

Cataclysmic variable stars (CVs) are an important class of post–common envelope binaries (PCEBs) in which a late-type main-sequence secondary star transfers matter to a white dwarf primary star via an accretion disk/column (Warner 1995). The majority of CVs have orbital periods of 80 minutes to 10 hr, and evolve toward shorter periods due to angular momentum losses (AMLs) through gravitational radiation (GR; Kraft et al. 1962; Paczyński 1967) and magnetic braking (MB; Verbunt & Zwaan 1981). If the orbital inclination is greater than 80°, the secondary star can obscure all other components and produce complex eclipse structures. In nonactivity states, the white dwarf eclipse can be separated by high-time-resolution observations. Therefore, in eclipsing CVs the white dwarf can also be timed precisely. Accurate eclipse timing measurements allow period variations to be studied, which can be used to detect the orbital evolution of CVs and circumbinary planets. Generally, secular period decreases derive from the system's AMLs via GR and MB. However, cyclic period oscillation can be the result of magnetic activity from the late-type secondary star (see Applegate 1992) or the light travel time effect (LTTE) from third-body perturbations (e.g., Qian et al. 2010a, 2011, 2015; Beuermann et al. 2011; Potter et al. 2011; Han et al. 2017). Applying the eclipse timing method, at least in principle, we can test the evolutionary theory of CVs and search for circumbinary companions around them.

Within the past decade, many circumbinary companions (e.g., planets or brown dwarfs) around CVs have been indirectly detected by eclipse timing variations, such as DP Leo (Qian et al. 2010b; Beuermann et al. 2011), UZ For (Potter et al. 2011; Khangale et al. 2019), HU Aqr (Qian et al. 2011; Goździewski et al. 2015), V893 Sco (Bruch 2014), OY Car (Han et al. 2015), V2051 Oph (Qian et al. 2015), DV UMa (Han et al. 2017), and SW Sex (Fang et al. 2020). An estimation method of the energy required to drive period fluctuations, presented by Brinkworth et al. (2006) and developed by Völschow et al. (2016), also has been used in these proposed circumbinary systems to exclude the Applegate mechanism. The result shows that such systems suffer from energy problems, with the exception of SW Sex. In addition, for supposedly multiplanet hosts (e.g., HU Aqr and UZ For),

the dynamical stability of the orbits has been analyzed and two-planet solutions have been found to be unstable (e.g., Horner et al. 2011; Potter et al. 2011; Hinse et al. 2012; Wittenmyer et al. 2012). Follow-up analysis by Goździewski et al. (2015), however, found that stable three-planet orbits for HU Aqr would be possible if the middle planet is in a retrograde orbit. More targets of ensured timing stability are required to understand the nature of eclipse timing variability, and many supposed planetary systems should also be constantly monitored on a long-term time baseline to test the prediction of previously proposed models.

As a dwarf-nova-type CV, HT Cas was first discovered as a U Gem star by Hoffmeister (1943). Subsequently, it was reclassified as an SU UMa–type star based on the detections of superhumps and rare, long, and irregular outbursts (e.g., Zhang et al. 1986; Wenzel 1987; Kato et al. 2012). Patterson (1981) presented an extensive photometric study that obtained the eclipsing light curves of HT Cas and estimated an orbital period of 1.77 hr. Due to its eclipse property, Horne et al. (1991) determined the well-constrained system parameters by modeling the eclipsing light curves. Also, the orbital ephemerides of HT Cas have been derived by many authors based on the continuously updated mid-eclipse times (Patterson 1981; Zhang et al. 1986; Horne et al. 1991; Mukai et al. 1997; Bruch 2000; Feline et al. 2005). However, they have found no evidence of period variations. Borges et al. (2008) presented new observations and detected a cyclic variation in the orbital period of HT Cas. However, the data coverage in this literature is only 0.8 times the proposed modulation period and it still needs more monitoring. In this paper, we present new eclipse timings of HT Cas spanning an additional 12 yr and update the $O-C$ diagram in order to study its orbital period changes. We describe the new observations in Section 2, and show an analysis of the eclipse timings in Section 3. A discussion on the physical causes of the eclipse timing variations is given in Section 4 and conclusions are provided in Section 5.

2. Observations and Data Reduction

HT Cas was observed with four different telescopes between 2008 October 19 and 2020 October 5: the Lijiang 2.4 m telescope equipped with a VersArray 1300B CCD camera from 2008 to 2011 and with the 2K × 4K YFOSC (Yunnan Faint Object Spectrograph and Camera) after 2012 and the Sino-Thai 70 cm reflecting telescope equipped with an Andor DW936N 2K CCD camera, located at the Lijiang observational station of Yunnan Observatories, and the 2.16 m and 85 cm telescopes at Xinglong Station administered by the National Astronomical Observatories, Chinese Academy of Sciences, mounted on which were the 1242 × 1152 BFOSC (Beijing Faint Object Spectrograph and Camera) detector and an Andor DW436 2K CCD camera, respectively. No filter was used for most of the observation. The V and R bands were used for several observations between 2008 October and 2009 July, and the others were obtained by using "no filter" in order to improve the time resolution further.

Data reduction was carried out by applying the aperture photometry package of the IRAF software after data preprocessing, including bias, dark, and flat-field corrections (see Tody 1986, 1993). We chose two nearby, no-variable stars as the comparison star and check star, and performed differential photometry procedures on the extracted original curves. Some sample eclipse profiles during quiescence are plotted in Figures 1 and 2. Note that there are two types of the quiescent eclipse light curves. The eclipse shape in Figure 1 exhibits white dwarf and bright spot eclipses (a two-step eclipse feature), but in Figure 2 the bright spot is very faint or absent. This behavior can be interpreted as the presence of quiescent high and low states in HT Cas that was previously reported by some authors (e.g., Berriman et al. 1987; Wood et al. 1995; Robertson & Honeycutt 1996; Feline et al. 2005), who concluded that the state changes are most likely the result of mass-transfer rate variation from the secondary star and through the accretion disk. Although the eclipse profiles are variable due to the effects of the accretion disk and hot spot, the ingress and egress times of the white dwarf are very stable. The earlier eclipse timings ($T_{\rm mid}$) were measured by averaging the mid-ingress (T_i) and mid-egress times (T_e) of the white dwarf eclipses, i.e., $T_{\rm mid}=(T_i+T_e)/2$. However, different methods were used to determine the mid-ingress and mid-egress times, such as the linear fitting method for both the ingress and egress branches of the white dwarf eclipses (Patterson 1981; Zhang et al. 1986) and the derivative technique described by Wood et al. (1985) (see Horne et al. 1991; Borges et al. 2008). The systematic error caused by the different methods is about 10 s (Horne et al. 1991). In the derivative method, T_i and T_e correspond to the minimum and maximum of points in the derivative curves. Therefore, we used this method to determine the mid-eclipse times of HT Cas. Two examples of measuring the mid-eclipse times of the white dwarf are displayed in Figure 3. With our observations during quiescence, we measured 31 new mid-eclipse times of the white dwarf by this method. The standard deviations in the measurement process were specified as the errors, which are closely connected with the data time resolution and signal-to-noise ratios. The measured mid-eclipse times and the errors are listed in Table 1. Besides these data, we found that a lot of quiescent light curves from the American Association of Variable Star Observers (AAVSO) database[11] are available for determining mid-eclipse times. Adopting the same method above, 92 mid-eclipse times were determined. Given that the reliability of the AAVSO data is significantly lower than that of our observations, the timing errors of the AAVSO data will be much larger. The eclipse timings derived from AAVSO are also listed in Table 1. We also converted all available mid-eclipse times to barycentric Julian dates in barycentric dynamical time (BJD_TDB).

3. Analysis of Eclipse Timing Variations

The orbital period of HT Cas has been studied previously and many eclipse timings have also been published (e.g., Patterson 1981; Zhang et al. 1986; Horne et al. 1991; Mukai et al. 1997; Bruch 2000; Feline et al. 2005; Borges et al. 2008). Due to the short observational baseline, the orbital period did not have any obvious changes before 2008. Later, Borges et al. (2008) reported that the orbital period may show a 36 yr cyclic period oscillation based on additional data. Based on the new mid-eclipse times presented in this paper and the previous eclipse times from the literature, the latest $O-C$ diagram of HT Cas was constructed by using the orbital ephemeris of

[11] https://www.aavso.org/LCGv2/

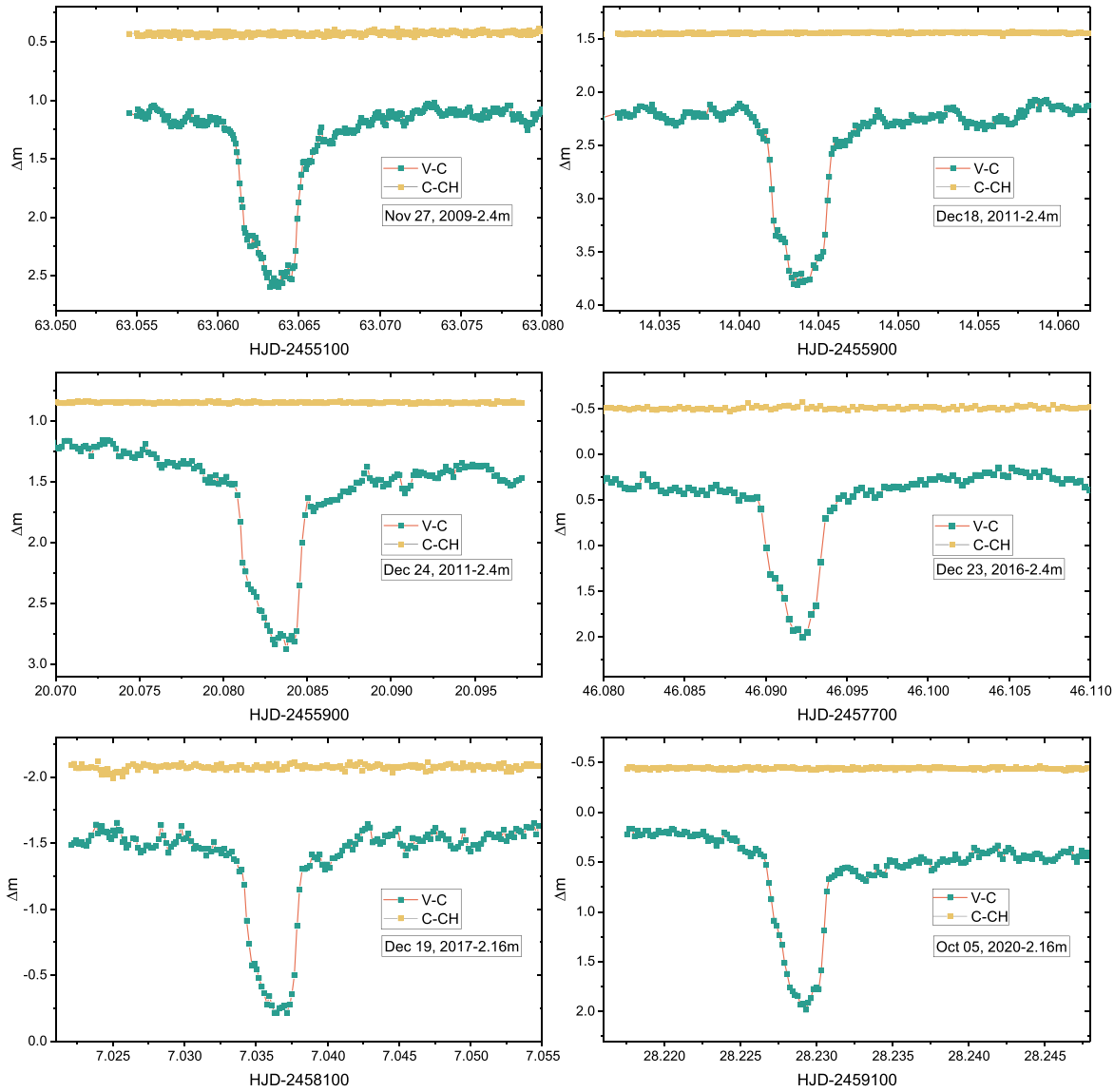

Figure 1. Six sample eclipse light curves of HT Cas during quiescence in the *N* band observed with 2.16 m and 2.4 m telescopes in China. The orange boxes refer to the magnitude differences between the comparison and check stars. The eclipse light curves display the properties of the white dwarf and bright spot eclipses.

Feline et al. (2005),

$$\begin{aligned}\text{Min.(BJD)} &= 2,443,727.937862(8)\\ &+ 0.07364720309(7) \times E,\end{aligned} \quad (1)$$

and is plotted in Figure 4. The updated $O-C$ curve has an observational baseline of ∼42 yr.

We noted that the new mid-eclipse times show significant departures from the model of Borges et al. (2008), being composed of the linear plus sinusoidal ephemeris. There appears to be a periodic variation in the $O-C$ curve (see top panel of Figure 4), and yet the sine curve is not sufficient to describe this change. In order to explore the possible cause of the cyclic fluctuation, we used an LTTE via the presence of a tertiary companion to replace the sinusoidal term. Therefore, the linear plus LTTE model was used to fit the $O-C$ curve, as follows:

$$(O-C)_1 = \Delta T_0 + \Delta P_0 \times E + \tau. \quad (2)$$

Here, ΔT_0 and ΔP_0 are the revision values of the initial epoch and orbital period, and τ is the LTTE perturbed by a tertiary component orbiting the eclipsing system (Irwin 1952, 1959):

$$\tau = A[(1-e^2)\frac{\sin(\nu+\omega)}{1+e\cos\nu} + e\sin\omega] \quad (3)$$

$$= A[\sqrt{1-e^2}\sin E^*\cos\omega + \cos E^*\sin\omega], \quad (4)$$

which includes five parameters of the LTTE orbit, i.e., A, e, ω, P_3, and T. Note that this equation does not contain both P_3 and T, which are the parameters related to E^*. A detailed explanation of these parameters can be found in Table 2 and in Han et al. (2017). Fitting results were obtained by applying the Levenberg–Marquardt method (Press et al. 1992) and are listed in Table 2. All timings were factored by weighting by the inverse of the squared errors. However, this model cannot sufficiently describe all observed timings, especially for cycle numbers between 79,770 and 125,129 (see Figure 4). Moreover, the most updated observations post-$E = 195{,}000$ (∼2017 December) show a departure from the predicted trend from this solution and the residuals seem to show significant deviations,

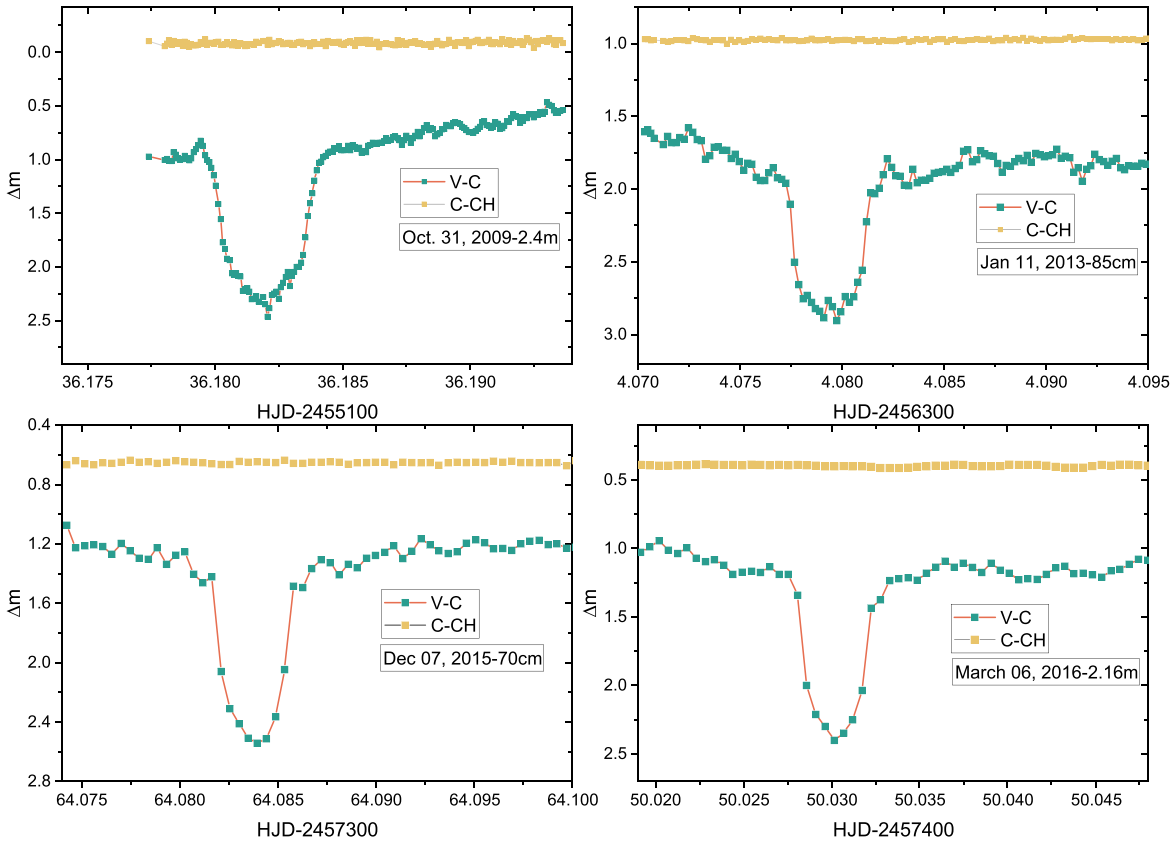

Figure 2. Four sample eclipse light curves of HT Cas during quiescence in the *N* band observed with 2.16 m, 2.4 m, 85 cm, and 70 cm telescopes in China. The orange boxes represent the magnitude differences between the comparison and check stars. The eclipse light curves show the lack of hot spots.

implying that a linear plus LTT ephemeris may not be a good solution. Adding a quadratic term to the ephemeris leads to a much better fit, as shown in Figure 5. The best-fitting ephemeris that describes the $O-C$ diagram can be represented as

$$(O\text{–}C)_2 = \Delta T_0 + \Delta P_0 \times E + \beta E^2 + \tau. \quad (5)$$

The same method was used to evaluate the fitting parameters, and the explanations of the parameters are the same as those in Table 2. The fit results with our best estimates of errors are also summarized in Table 2. The quadratic plus LTT ephemeris results in a smaller reduced $\chi^2 = 0.0003$ and residual sum of squares $\delta^2 = 2.09 \times 10^{-6}$ than those of the linear plus LTT model ($\chi^2 = 0.0008$ and $\delta^2 = 2.89 \times 10^{-6}$). Additionally, a method of variance analysis (i.e., an *F*-test; Pringle 1975) was applied to assess whether the quadratic term is significant, and the *F*-statistic values are also listed in Table 2. All these results show that a quadratic plus LTT ephemeris is a better model with a higher level of confidence (>99.99%). Also note that this conclusion is only based on the existing data, which just cover 1.25 orbital cycles and lack the pre-1978 timings. Thus, there may be a systematic error of several years. But how to find this error is a complex problem and we require more monitoring.

The downward parabola in Figure 5 reveals a secular decay in the orbital period at a rate of $\dot{P} = -9.72 \times 10^{-14}$days/cycle $= -1.32 \times 10^{-12}$ ss^{-1}. Additionally, the orbital period of HT Cas shows a periodic wiggle with an amplitude of 79.3 s and a period of 30.28 yr. In Figure 5, the orange solid lines in the top and middle panels are the theoretical orbit of a hypothetical third body orbiting HT Cas, and the blue dashed line in the upper panel represents the quadratic term of the best-fitting model. The residuals from such a model are plotted in the bottom panel.

4. Results and Discussion

4.1. Interpretations of Secular Period Variation

4.1.1. Intrinsic AML Mechanisms: GR and MB

The long-term evolution of CVs is the result of AMLs. In long-period systems ($P_{\rm orb} \geqslant 3$ hr), the dominant AML mechanism is the magnetized stellar wind, or MB (e.g., Verbunt & Zwaan 1981), whereas short-period systems ($P_{\rm orb} \leqslant 2$ hr) are considered to be driven entirely by GR (e.g., Paczyński 1967; Faulkner 1971; Landau & Lifshitz 1975). HT Cas is a short-period CV with an orbital period of ∼1.77 hr, consisting of a white dwarf and a fully convective M-type star. Hence, the observed period decrease in HT Cas can be the result of systemic AML due to GR. The orbital period decrease rate from gravitational waves is

$$\frac{\dot{P}_{\rm GR}}{P_{\rm orb}} = -3\frac{32G^3}{5c^5}\frac{M_1M_2(M_1+M_2)}{a^4}, \quad (6)$$

where a and c are the orbital separation and the speed of light, respectively. Applying the binary parameters ($M_1 = 0.61M_\odot$, $M_2 = 0.09M_\odot$, and $a = 0.658R_\odot$) from Horne et al. (1991), we calculated the GR-driven period decrease rate to be $\dot{P}_{\rm GR} = -1.03 \times 10^{-13}$ ss^{-1}, which is 1 order of magnitude

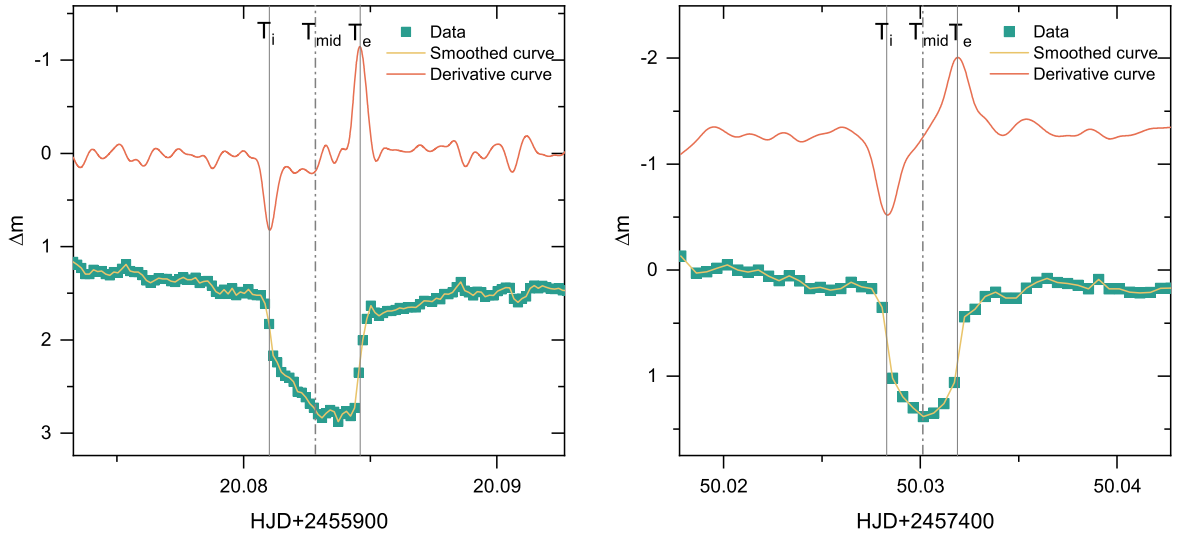

Figure 3. Two examples of determining mid-eclipse times for two different types of the quiescent curve. The cyan boxes represent the light curves, and the yellow solid curves are the corresponding smoothed light curves. The derivative curves are plotted in the upper part of the diagrams. The vertical solid lines refer to the mid-ingress (T_i) and mid-egress times (T_e) of the white dwarf, while the dashed–dotted lines denote the mid-eclipse times ($T_{\rm mid}$).

lower than the observed value. Therefore, other AML mechanisms are required to produce the secular decrease.

The standard model of CV evolution assumes the cessation of MB when the donor loses its radiative core (e.g., Rappaport et al. 1983; Spruit & Ritter 1983). However, many studies have shown that fully convective stars still have intense stellar magnetic activity (e.g., Fleming et al. 1995; Hodgkin et al. 1995; Linsky et al. 1995; Delfosse et al. 1998), and they are capable of producing substantial magnetic fields (e.g., Saar & Linsky 1985; Johns-Krull & Valenti 1996; Reiners & Basri 2007; Morin et al. 2008). A recent study found that MB is not disrupted at an orbital period of ∼3 hr but reduces fast enough (Garraffo et al. 2018). Therefore, MB-driven AML should not be ignored below the period gap. To calculate the orbital period decrease due to MB, we adopted the MB prescription proposed by Rappaport et al. (1983),

$$\dot{P}_{\rm MB} = -1.4 \times 10^{-12}\left(\frac{M_\odot}{M_1}\right)\left(\frac{M_1+M_2}{M_\odot}\right)^{1/3} \times \left(\frac{R_2}{R_\odot}\right)^{\gamma}\left(\frac{d}{P_{\rm orb}}\right)^{7/3} {\rm ss}^{-1}, \quad (7)$$

where R_2 is the donor's radius, and γ is the MB index in the range of 0 to 4. Using the radius $R_2 = 0.154R_\odot$ (Horne et al. 1991) and the standard value of $\gamma = 4$, we derived the period decay rate via MB to be $\dot{P}_{\rm MB} = -5.88 \times 10^{-14}\,{\rm ss}^{-1}$. This value is 2 orders of magnitude smaller than the observed one. Moreover, Garraffo et al. (2018) found a fast decrease in MB (∼90%) when the orbital period is close to 3.2 hr and below the gap $\dot{P}_{\rm MB} \sim \dot{P}_{\rm GR}/100$. This implies that the residual MB is not strong enough to play a dominant role in the evolution of HT Cas. Consequently, there should be some other AML mechanisms at work besides GR and MB.

4.1.2. Additional AML Mechanisms

The revised model of CV evolution presented by Knigge et al. (2011) shows that below the period gap the AML rate is about 2.47 times the GR-induced AML rate, indicating that there should be additional AML mechanisms. Under this model, many discrepancies between theory and observations could be solved, such as the period distribution, space density, and minimum period. In fact, the consequential AML (CAML) mechanism, caused by the mass transfer during the binary evolution, has been proposed a few decades ago (Webbink 1985; King & Kolb 1995). To explain the origin of extra AMLs, Schenker et al. (1998) studied the effect of friction between the secondary star and the expanding nova shell after a nova explosion. However, this model was unable to reproduce the observed period distribution. Recently, Schreiber et al. (2016) proposed an empirical CAML (eCAML) model in which the specific angular momentum of the lost matter increases with decreasing white dwarf mass, and found that this model can solve several points of disagreement between predictions and observations, especially the white dwarf mass problem in CVs. The eCAML model has been supported by new observational evidence (see Pala et al. 2022). As shown in Pala et al. (2022), there is an anticorrelation between the average accretion rates and the white dwarf masses for short-period CVs, which suggests the presence of an extra AML mechanism that has a major influence on the evolution of CVs with low white dwarf masses. We used the eCAML model from Schreiber et al. (2016) to estimate the orbital period decrease due to CAML,

$$\frac{\dot{P}_{\rm CAML}}{P_{\rm orb}} = -3 \times \frac{0.35}{M_1}\frac{\dot{M}_2}{M_2}, \quad (8)$$

where $\dot{M}_2$ is the mass accretion rate. Adopting the parameter $\dot{M}_2 = 2.2 \times 10^{-10} M_\odot {\rm yr}^{-1}$ from Pala et al. (2022), we derived the period decay rate to be $\dot{P}_{\rm CAML} = -8.48 \times 10^{-13}\,{\rm ss}^{-1}$. Note that the total AML rate from the system is $\dot{J} = \dot{J}_{\rm sys} + \dot{J}_{\rm CAML}$, so the total period decrease rate should be $\dot{P}_{\rm total} = \dot{P}_{\rm GR} + \dot{P}_{\rm MB} + \dot{P}_{\rm CAML} \simeq -1.01 \times 10^{-12}\,{\rm ss}^{-1}$, which is very close to the observed value $\dot{P}$. Therefore, we argue that the observed period decrease in HT Cas could be explained if additional AML mechanisms are taken into account.

However, the eCAML model is purely empirical and still lacks the exact physical mechanism. Several different physical

Table 1
New Mid-eclipse Times of HT Cas

Date	Min. (HJD)	Min. (BJD)	Epoch	$O-C$	Err.	Telescope	Filter
2008 Oct 19	2,454,759.18225	2,454,759.18301	149,785	−0.00116	0.00010	85 cm	*N*
2008 Nov 10	2,454,781.20250	2,454,781.20326	150,084	−0.00143	0.00010	85 cm	*V*
2008 Nov 25	2,454,796.15320	2,454,796.15396	150,287	−0.00111	0.00005	2.4 m	*N*
2008 Nov 28	2,454,799.02528	2,454,799.02604	150,326	−0.00128	0.00005	2.4 m	*N*
2008 Dec 25	2,454,816.03768	2,454,816.03844	150,557	−0.00138	0.00010	85 cm	*R*
2009 Jan 15	2,454,847.04335	2,454,847.04412	150,978	−0.00117	0.00005	2.4 m	*V*
2009 Jan 21	2,454,853.00880	2,454,853.00957	151,059	−0.00114	0.00005	2.4 m	*R*
2009 Jul 1	2,455,014.22224	2,455,014.22301	153,248	−0.00143	0.00010	85 cm	*R*
2009 Oct 31	2,455,136.18195	2,455,136.18271	154,904	−0.00150	0.00005	2.4 m	*N*
2009 Nov 27	2,455,163.06322	2,455,163.06398	155,269	−0.00145	0.00005	2.4 m	*N*
2010 Jan 14	2,455,211.15476	2,455,211.15553	155,922	−0.00154	0.00005	2.4 m	*N*
2010 Nov 30	2,455,531.15205	2,455,531.15281	160,267	−0.00135	0.00005	2.4 m	*N*
2011 Dec 18	2,455,914.04378	2,455,914.04453	165,466	−0.00144	0.00005	2.4 m	*N*
2011 Dec 24	2,455,920.08281	2,455,920.08357	165,548	−0.00147	0.00005	2.4 m	*N*
2011 Dec 31	2,455,927.07928	2,455,927.08003	165,643	−0.00149	0.00005	2.4 m	*N*
2012 Oct 4	2,456,204.80313	2,456,204.80390	169,414	−0.00123	0.00010	AAVSO	*V*
2012 Oct 7	2,456,207.89627	2,456,207.89704	169,456	−0.00127	0.00020	AAVSO	*V*
2012 Oct 15	2,456,215.77621	2,456,215.77697	169,563	−0.00159	0.00020	AAVSO	*V*
2012 Oct 16	2,456,216.88100	2,456,216.88176	169,578	−0.00150	0.00020	AAVSO	*V*
2012 Oct 17	2,456,217.76500	2,456,217.76577	169,590	−0.00127	0.00020	AAVSO	*V*
2012 Oct 18	2,456,218.79593	2,456,218.79670	169,604	−0.00140	0.00020	AAVSO	*V*
2012 Oct 18	2,456,218.86938	2,456,218.87015	169,605	−0.00159	0.00020	AAVSO	*V*
2012 Oct 20	2,456,220.85793	2,456,220.85870	169,632	−0.00152	0.00020	AAVSO	*V*
2012 Oct 26	2,456,226.89715	2,456,226.89792	169,714	−0.00137	0.00010	AAVSO	*V*
2012 Oct 29	2,456,229.84297	2,456,229.84374	169,754	−0.00144	0.00020	AAVSO	*V*
2012 Dec 2	2,456,263.57329	2,456,263.57406	170,212	−0.00154	0.00010	AAVSO	*V*
2012 Dec 2	2,456,263.64711	2,456,263.64788	170,213	−0.00137	0.00010	AAVSO	*V*
2012 Dec 2	2,456,263.72069	2,456,263.72145	170,214	−0.00143	0.00010	AAVSO	*V*
2012 Dec 2	2,456,263.79437	2,456,263.79514	170,215	−0.00140	0.00010	AAVSO	*V*
2012 Dec 2	2,456,263.86785	2,456,263.86861	170,216	−0.00157	0.00010	AAVSO	*V*
2012 Dec 3	2,456,264.60441	2,456,264.60517	170,226	−0.00148	0.00010	AAVSO	*V*
2012 Dec 3	2,456,264.67823	2,456,264.67900	170,227	−0.00130	0.00020	AAVSO	*V*
2012 Dec 3	2,456,264.75176	2,456,264.75253	170,228	−0.00142	0.00020	AAVSO	*V*
2012 Dec 3	2,456,264.82550	2,456,264.82627	170,229	−0.00133	0.00020	AAVSO	*V*
2012 Dec 4	2,456,265.56206	2,456,265.56283	170,239	−0.00124	0.00020	AAVSO	*V*
2012 Dec 4	2,456,265.63552	2,456,265.63629	170,240	−0.00143	0.00020	AAVSO	*V*
2012 Dec 4	2,456,265.70908	2,456,265.70985	170,241	−0.00151	0.00020	AAVSO	*V*
2012 Dec 4	2,456,265.78271	2,456,265.78348	170,242	−0.00153	0.00020	AAVSO	*V*
2012 Dec 4	2,456,265.85644	2,456,265.85720	170,243	−0.00145	0.00020	AAVSO	*V*
2012 Dec 8	2,456,269.61237	2,456,269.61313	170,294	−0.00153	0.00020	AAVSO	*V*
2012 Dec 8	2,456,269.75983	2,456,269.76059	170,296	−0.00137	0.00020	AAVSO	*V*
2012 Dec 8	2,456,269.83322	2,456,269.83399	170,297	−0.00162	0.00020	AAVSO	*V*
2012 Dec 9	2,456,270.86461	2,456,270.86537	170,311	−0.00129	0.00020	AAVSO	*V*
2013 Jan 11	2,456,304.07932	2,456,304.08009	170,762	−0.00147	0.00010	85 cm	*N*
2013 Sep 9	2,456,545.42137	2,456,545.42214	174,039	−0.00130	0.00020	AAVSO	*V*
2015 Nov 21	2,457,348.17583	2,457,348.17663	184,939	−0.00133	0.00010	85 cm	*N*
2015 Nov 23	2,457,350.09079	2,457,350.09160	184,965	−0.00119	0.00010	85 cm	*N*
2015 Dec 4	2,457,360.99034	2,457,360.99114	185,113	−0.00143	0.00010	85 cm	*N*
2015 Dec 7	2,457,364.08370	2,457,364.08450	185,155	−0.00125	0.00010	70 cm	*N*
2015 Dec 10	2,457,367.02943	2,457,367.03023	185,195	−0.00140	0.00010	85 cm	*N*
2016 Jan 6	2,457,394.05815	2,457,394.05896	185,562	−0.00121	0.00005	2.16 m	*N*
2016 Feb 5	2,457,424.03237	2,457,424.03317	185,969	−0.00140	0.00005	2.4 m	*N*
2016 Mar 2	2,457,450.02989	2,457,450.03069	186,322	−0.00135	0.00005	2.16 m	*N*
2016 Dec 23	2,457,746.09166	2,457,746.09247	190,342	−0.00132	0.00005	2.4 m	*N*
2017 Jan 29	2,457,783.06240	2,457,783.06322	190,844	−0.00147	0.00010	70 cm	*N*
2017 Oct 31	2,458,058.35588	2,458,058.35671	194,582	−0.00123	0.00020	AAVSO	*V*
2017 Nov 5	2,458,063.43746	2,458,063.43828	194,651	−0.00131	0.00010	AAVSO	*V*
2017 Nov 6	2,458,064.32120	2,458,064.32202	194,663	−0.00134	0.00010	AAVSO	*V*
2017 Nov 6	2,458,064.39468	2,458,064.39550	194,664	−0.00151	0.00010	AAVSO	*V*
2017 Nov 6	2,458,064.46835	2,458,064.46917	194,665	−0.00148	0.00010	AAVSO	*V*
2017 Nov 7	2,458,065.35232	2,458,065.35315	194,677	−0.00127	0.00010	AAVSO	*V*
2017 Nov 8	2,458,066.45697	2,458,066.45780	194,692	−0.00133	0.00010	AAVSO	*V*
2017 Nov 11	2,458,069.40295	2,458,069.40377	194,732	−0.00124	0.00020	AAVSO	*V*
2017 Nov 11	2,458,069.47650	2,458,069.47733	194,733	−0.00134	0.00020	AAVSO	*V*

Table 1
(Continued)

Date	Min. (HJD)	Min. (BJD)	Epoch	$O - C$	Err.	Telescope	Filter
2017 Nov 12	2,458,069.55018	2,458,069.55101	194,734	−0.00130	0.00020	AAVSO	*V*
2017 Nov 12	2,458,069.62388	2,458,069.62470	194,735	−0.00126	0.00010	AAVSO	*V*
2017 Nov 12	2,458,070.28657	2,458,070.28739	194,744	−0.00139	0.00010	AAVSO	*V*
2017 Nov 12	2,458,070.36034	2,458,070.36117	194,745	−0.00126	0.00020	AAVSO	*V*
2017 Nov 13	2,458,071.39122	2,458,071.39205	194,759	−0.00144	0.00010	AAVSO	*V*
2017 Nov 13	2,458,071.46507	2,458,071.46589	194,760	−0.00124	0.00020	AAVSO	*V*
2017 Nov 14	2,458,071.53869	2,458,071.53951	194,761	−0.00127	0.00020	AAVSO	*V*
2017 Nov 14	2,458,071.61229	2,458,071.61311	194,762	−0.00132	0.00020	AAVSO	*V*
2017 Nov 14	2,458,072.34883	2,458,072.34965	194,772	−0.00125	0.00020	AAVSO	*V*
2017 Nov 14	2,458,072.42245	2,458,072.42328	194,773	−0.00127	0.00010	AAVSO	*V*
2017 Nov 14	2,458,072.49608	2,458,072.49691	194,774	−0.00129	0.00010	AAVSO	*V*
2017 Nov 15	2,458,072.56965	2,458,072.57047	194,775	−0.00137	0.00010	AAVSO	*V*
2017 Nov 15	2,458,073.30611	2,458,073.30693	194,785	−0.00138	0.00010	AAVSO	*V*
2017 Nov 15	2,458,073.37983	2,458,073.38065	194,786	−0.00132	0.00010	AAVSO	*V*
2017 Nov 15	2,458,073.45359	2,458,073.45441	194,787	−0.00120	0.00020	AAVSO	*V*
2017 Nov 16	2,458,073.52711	2,458,073.52793	194,788	−0.00133	0.00010	AAVSO	*V*
2017 Nov 16	2,458,073.60077	2,458,073.60160	194,789	−0.00131	0.00010	AAVSO	*V*
2017 Nov 16	2,458,074.33750	2,458,074.33832	194,799	−0.00106	0.00010	AAVSO	*V*
2017 Nov 16	2,458,074.41081	2,458,074.41163	194,800	−0.00139	0.00010	AAVSO	*V*
2017 Nov 16	2,458,074.48451	2,458,074.48534	194,801	−0.00133	0.00010	AAVSO	*V*
2017 Nov 17	2,458,074.55801	2,458,074.55884	194,802	−0.00148	0.00010	AAVSO	*V*
2017 Nov 17	2,458,075.29469	2,458,075.29551	194,812	−0.00128	0.00010	AAVSO	*V*
2017 Nov 18	2,458,075.51561	2,458,075.51644	194,815	−0.00130	0.00010	AAVSO	*V*
2017 Nov 18	2,458,075.58925	2,458,075.59007	194,816	−0.00131	0.00020	AAVSO	*V*
2017 Nov 18	2,458,076.32588	2,458,076.32670	194,826	−0.00115	0.00010	AAVSO	*V*
2017 Nov 18	2,458,076.39938	2,458,076.40020	194,827	−0.00130	0.00010	AAVSO	*V*
2017 Nov 18	2,458,076.47294	2,458,076.47376	194,828	−0.00139	0.00010	AAVSO	*V*
2017 Nov 19	2,458,076.62038	2,458,076.62120	194,830	−0.00124	0.00010	AAVSO	*V*
2017 Nov 19	2,458,077.28305	2,458,077.28387	194,839	−0.00139	0.00010	AAVSO	*V*
2017 Nov 19	2,458,077.35660	2,458,077.35742	194,840	−0.00149	0.00010	AAVSO	*V*
2017 Nov 19	2,458,077.43036	2,458,077.43118	194,841	−0.00138	0.00010	AAVSO	*V*
2017 Nov 20	2,458,077.50414	2,458,077.50496	194,842	−0.00125	0.00010	AAVSO	*V*
2017 Dec 19	2,458,107.03635	2,458,107.03717	195,243	−0.00156	0.00005	2.16 m	*N*
2017 Dec 20	2,458,107.92028	2,458,107.92111	195,255	−0.00139	0.00005	2.16 m	*N*
2017 Dec 27	2,458,115.06403	2,458,115.06485	195,352	−0.00143	0.00005	2.4 m	*N*
2018 Nov 3	2,458,425.63439	2,458,425.63521	199,569	−0.00132	0.00010	AAVSO	*V*
2018 Nov 3	2,458,425.92885	2,458,425.92967	199,573	−0.00145	0.00010	AAVSO	*V*
2018 Nov 23	2,458,445.59253	2,458,445.59335	199,840	−0.00158	0.00010	AAVSO	*V*
2018 Dec 8	2,458,460.61672	2,458,460.61754	200,044	−0.00142	0.00010	AAVSO	*V*
2018 Dec 9	2,458,461.64788	2,458,461.64870	200,058	−0.00132	0.00010	AAVSO	*V*
2018 Dec 10	2,458,462.60512	2,458,462.60594	200,071	−0.00149	0.00010	AAVSO	*V*
2018 Dec 10	2,458,462.67885	2,458,462.67967	200,072	−0.00141	0.00010	AAVSO	*V*
2018 Dec 10	2,458,462.75234	2,458,462.75316	200,073	−0.00156	0.00010	AAVSO	*V*
2018 Dec 11	2,458,463.56243	2,458,463.56325	200,084	−0.00160	0.00010	AAVSO	*V*
2018 Dec 11	2,458,463.63609	2,458,463.63692	200,085	−0.00158	0.00010	AAVSO	*V*
2018 Dec 11	2,458,463.70995	2,458,463.71077	200,086	−0.00137	0.00010	AAVSO	*V*
2018 Dec 18	2,458,471.44290	2,458,471.44372	200,191	−0.00138	0.00010	AAVSO	*V*
2018 Dec 19	2,458,471.51643	2,458,471.51725	200,192	−0.00149	0.00010	AAVSO	*V*
2019 Jan 23	2,458,506.64642	2,458,506.64724	200,669	−0.00122	0.00010	AAVSO	*V*
2019 Jan 23	2,458,506.71985	2,458,506.72067	200,670	−0.00144	0.00010	AAVSO	*V*
2019 Jan 28	2,458,511.65427	2,458,511.65509	200,737	−0.00138	0.00010	AAVSO	*V*
2019 Jan 28	2,458,511.72785	2,458,511.72867	200,738	−0.00145	0.00010	AAVSO	*V*
2019 Jan 30	2,458,513.64267	2,458,513.64349	200,764	−0.00145	0.00010	AAVSO	*V*
2019 Jan 30	2,458,513.71626	2,458,513.71708	200,765	−0.00151	0.00010	AAVSO	*V*
2019 Feb 8	2,458,522.62766	2,458,522.62847	200,886	−0.00143	0.00010	AAVSO	*V*
2019 Feb 8	2,458,522.70092	2,458,522.70173	200,887	−0.00182	0.00010	AAVSO	*V*
2020 Sep 27	2,459,120.12895	2,459,120.12975	208,999	−0.00153	0.00010	85 cm	*N*
2020 Oct 5	2,459,128.22850	2,459,128.22930	209,109	−0.00155	0.00005	2.16 m	*N*
2021 Jun 19	2,459,384.66820	2,459,384.668994	212,591	−0.00142	0.00010	AAVSO	*V*

(This table is available in machine-readable form.)

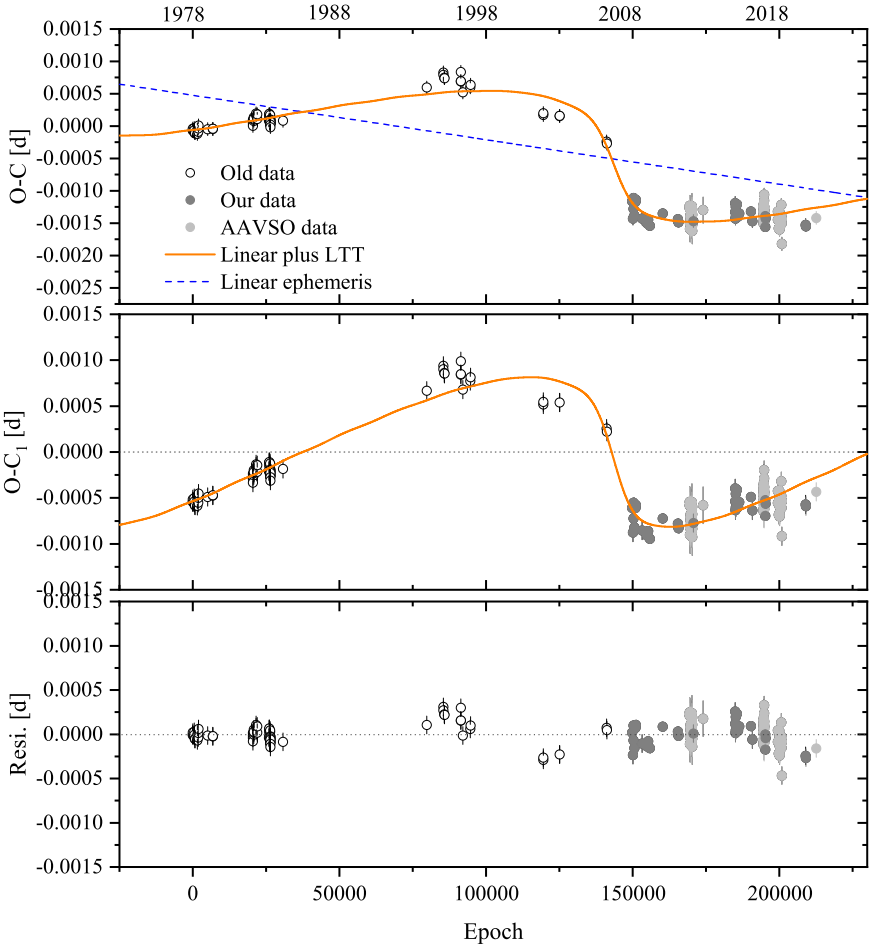

Figure 4. Latest $O-C$ diagram of HT Cas constructed with a linear plus light travel time (LTT) ephemeris. The black open circles denote all historical timings, while the dark gray solid circles refer to our eclipse timings and the light gray solid circles denote the AAVSO data. The orange solid line in the top panel represents the best-fit model. The middle panel shows the LTTE orbit and the bottom panel displays the fit residuals from the complete ephemeris.

origins for CAML have been proposed in the literature, such as the presence of a circumbinary disk (van den Heuvel 1994; Taam & Spruit 2001), a fast isotropic wind from the white dwarf (King & Kolb 1995), the outflows from the Lagrangian points (Vanbeveren 1998), and the friction during nova eruptions (Schenker et al. 1998). Shao & Li (2012) discussed several potential possibilities of the CAML mechanisms, and found that the outflows from an outer Lagrangian point or a circumbinary disk can account for the additional AML below the period gap. But several recent studies showed that the best candidate for CAML is the friction between the system and a nova shell around it (Nelemans et al. 2016; Schreiber et al. 2016; Sparks & Sion 2021), possibly resembling a circumbinary disk formed from the remaining ejected material in a nova eruption (see Liu & Li 2016), or a common envelope phase (see Nelemans et al. 2016; Liu & Li 2019). To evaluate the AML rate from nova eruption, we considered the AML to be a continuous process and to be similar to that of a circumbinary toroid/disk. The period decrease rate due to the friction during nova eruptions is given by (Nelemans et al. 2016)

$$\frac{\dot{P}_{\rm Nova}}{P_{\rm orb}} = -3\alpha\frac{\dot{M}_2}{M_2}\left[1+q+\frac{q^2}{2(1+q)}\right]. \quad (9)$$

where $q = M_2/M_1$ is the mass ratio, and the parameter α is the ratio of the mass-loss rate from the system to the mass-transfer rate ($\alpha = \dot{M}_{\rm ej}/\dot{M}_2$). We generally assume that all of the material accreted by the white dwarf is ejected during nova eruptions, i.e., $\alpha = 1$ (Knigge et al. 2011). For HT Cas, the period decrease rate via nova eruptions can be estimated as $\dot{P}_{\rm Nova} = -1.71 \times 10^{-12}\,{\rm ss}^{-1}$. As expected, this value is slightly larger than both the observed value $\dot{P}$ and the predicted value $\dot{P}_{\rm total}$ above owing to the assumption of a nova ejecta fraction of 100%. Finally, we conclude that the eCAML model is in good agreement with the observed period decay in HT Cas and the physical cause behind eCAML most likely originates from the friction between the secondary star and the ejecta during nova explosions.

We still cannot completely rule out the possibility that the secular orbital decay in HT Cas could be only a part of a very-long-period cyclic fluctuation as a result of the LTTE in the presence of a wider-orbit companion. To test this hypothesis, the system will require more monitoring to expand the data coverage in the future.

4.2. Cyclic Period Variation

4.2.1. LTTE and Applegate Mechanism

Cyclic period modulations are observed in many PCEBs, and can be interpreted as the magnetic activity cycle in M dwarfs, i.e., the so-called Applegate mechanism (Applegate 1992), or as

Table 2
Orbital Parameters of the Circumbinary Giant Planet in HT Cas

Parameters	Linear plus LTTE	Quadratic plus LTTE	Units
ΔT_0	+4.76	+4.65	days
	$(\pm 1.26) \times 10^{-4}$	$(\pm 0.42) \times 10^{-4}$	
ΔP_0	−6.87	−4.03	days
	$(\pm 0.90) \times 10^{-9}$	$(\pm 0.86) \times 10^{-10}$	
β	⋯	−9.72	days/
		$(\pm 0.85) \times 10^{-14}$	cycle
e	0.81 (± 0.04)	0.82 (± 0.05)	⋯
ω	3.24 (± 0.04)	3.71 (± 0.08)	deg
T	2,440,048.87	2,443,737.16	BJD
	(± 963.99)	(± 69.86)	
A	0.001391	0.000918	days
	(± 0.000189)	(± 0.000095)	
P_3	39.13 (± 2.61)	30.28 (± 0.13)	yr
$a_{12} \sin i'$	0.241 (± 0.033)	0.159 (± 0.016)	au
$f(m)$	$9.13 (\pm 3.92) \times 10^{-6}$	$4.38 (\pm 1.35) \times 10^{-6}$	$M_\odot$
$M_3 \sin i'$	0.017 (± 0.004)	0.013 (± 0.002)	$M_\odot$
d_3 $(i' = 90°)$	11.97 (± 3.22)	10.13 (± 2.07)	au
δ^2	2.89×10^{-6}	2.09×10^{-6}	⋯
λ	7318.50	10,077.65	⋯
χ^2	0.0008	0.0003	⋯

Note. ΔT_0—revised epoch; ΔP_0—revised orbital period; β—rate of linear period decrease; e—eccentricity; ω—longitude of periastron passage; T—periastron passage; A—semiamplitude; P_3—orbital period of the third companion; $a_{12} \sin i'$—projected semimajor axis; $f(m)$—mass function; $M_3 \sin i'$—mass of the third companion; d_3—orbital separation; δ^2—residual sum of squares; λ—F-statistic value; χ^2—chi-square.

the LTTE due to the perturbation of potential Jupiter-like planets. To test whether the eclipse timing variations in PCEBs could be caused by magnetic activity, some previous authors have calculated the energy required to produce the change via Applegate's mechanism. More specifically, the required energy for the change is compared to the energy that is produced by the star. In the case of HT Cas, we first used an approach from Brinkworth et al. (2006) to estimate the energy required of Applegate's mechanism. The result shows that the energy requirement is slightly higher than the maximum available energy of the star (see Figure 6). In our analysis, we applied 2500 K for a donor star of $\sim 0.09 M_\odot$ to estimate its luminosity by $L_2 = \left(\frac{R_2}{R_\odot}\right)^2 \left(\frac{T_2}{T_\odot}\right)^2 L_\odot$. Völschow et al. (2016) further improved the Brinkworth et al. (2006) model by considering the angular momentum exchange between a finite shell and the core of the donor star. A publicly available *Applegate calculator*[12] based on this framework could also be employed to assess the energetic feasibility of the Applegate mechanism. Based on the calculations, we show that the lower limit of the required energy divided by the available energy is $\Delta E / E_{\rm sec} \sim 0.91$, which means that HT Cas requires a substantial fraction of the available energy, although still less than 100%. In addition, those authors found that Applegate's mechanism becomes more feasible with increasing donor mass and decreasing orbital separation, and an ideal Applegate candidate is a system with a tight orbit of $\sim 0.5 R_\odot$ and a donor star of $\sim 0.5 M_\odot$. More recently, the most detailed approach described so far was proposed by Völschow et al. (2018), who suggested that the most promising Applegate PCEBs are low-mass systems with binary separations $\leqslant 1 R_\odot$ and donor masses in the range of 0.30–$0.36 M_\odot$. Besides, a study by Ak et al. (2001) found that the solar-type activity cycles for the secondary star in short-period CVs have a peak value at 9.7 yr, which is obviously shorter than the observed oscillation period of ∼30.28 yr. These imply that magnetic activity is probably not the dominant mechanism here, and the third-body model seems to be more feasible. Nevertheless, the Applegate process should not be entirely neglected when analyzing the $O - C$ curve of HT Cas as it could contribute to additional scatter.

In the framework of third-body hypothesis, we derived the mass of the tertiary component as $M_3 \sin i' = 0.013(\pm 0.002) M_\odot = 13.61(\pm 2.09) M_{\rm Jup}$ by using the best-fitting parameters listed in Table 2 and the binary parameters from Horne et al. (1991). Assuming coplanarity between the tertiary companion and the eclipsing host star (i.e., $i' = i = 81°$), the third body's mass would match a giant planet's, at an orbital separation of ∼10.13 au in a very high eccentricity orbit ($e = 0.82$). We have examined all supposed circumbinary planetary PCEBs and found that this extreme eccentricity is second only to that of the highly eccentric planet in QS Vir (Almeida & Jablonski 2011). Horner et al. (2011) showed, however, that a system with two extra bodies is dynamically unstable. The most recent data from Bours et al. (2016) also showed that the eclipse time variations in QS Vir are very complex, and what causes them is still unknown. Therefore, HT Cas could be a very interesting triple system with a highly eccentric planetary orbit.

4.2.2. Applegate–Lanza Mechanism

More recently, an Applegate-like mechanism was proposed to explain orbital period modulation in close binaries with a late-type magnetically active donor (Lanza 2020). This model supposes that a persistent nonaxisymmetric internal magnetic field results in a nonaxisymmetric component of the gravitational quadrupole moment of the active star. The spin angular momentum of the active component is coupled with the orbital angular momentum, and ultimately causes the modulation of the orbital period. Here we apply Lanza's model to test whether the cyclic period variation in HT Cas may result from the Applegate-like process.

The relative amplitude of the variation of the donor's angular velocity is given by (Lanza 2020, Equation (56))

$$\frac{\Delta \Omega}{\Omega} = -\frac{ma^2}{3I_s} \frac{\Delta P}{P}, \tag{10}$$

where m and a are the reduced mass and the semimajor axis of the binary, respectively. I_s is the moment of inertia of the donor star about the spin axis, and $\Delta P / P = \Delta t / T$ is the relative amplitude of the period modulation, or equivalently the $O - C$ deviations Δt over the timescale T of the $O - C$ curve. The consequent variation in rotational energy is

$$\Delta E_{\rm rot} = I_s \Omega \Delta \Omega = -[m r_0^2 \Omega^2] \frac{\Delta t}{3T}. \tag{11}$$

For HT Cas, the relative amplitude of the period modulation is $\Delta P / P \approx 5.22 \times 10^{-7}$, i.e., $\Delta t / 3T = 1.74 \times 10^{-7}$. The reduced mass is $m = 0.078 M_\odot$, and the angular velocity is $\Omega = 2\pi / P_{\rm orb} = 9.87 \times 10^{-4}$ s^{-1}. The orbital radius is usually the semimajor axis length of the secondary star ($r_0 = a_2$).

[12] http://theory-starformation-group.cl/applegate/

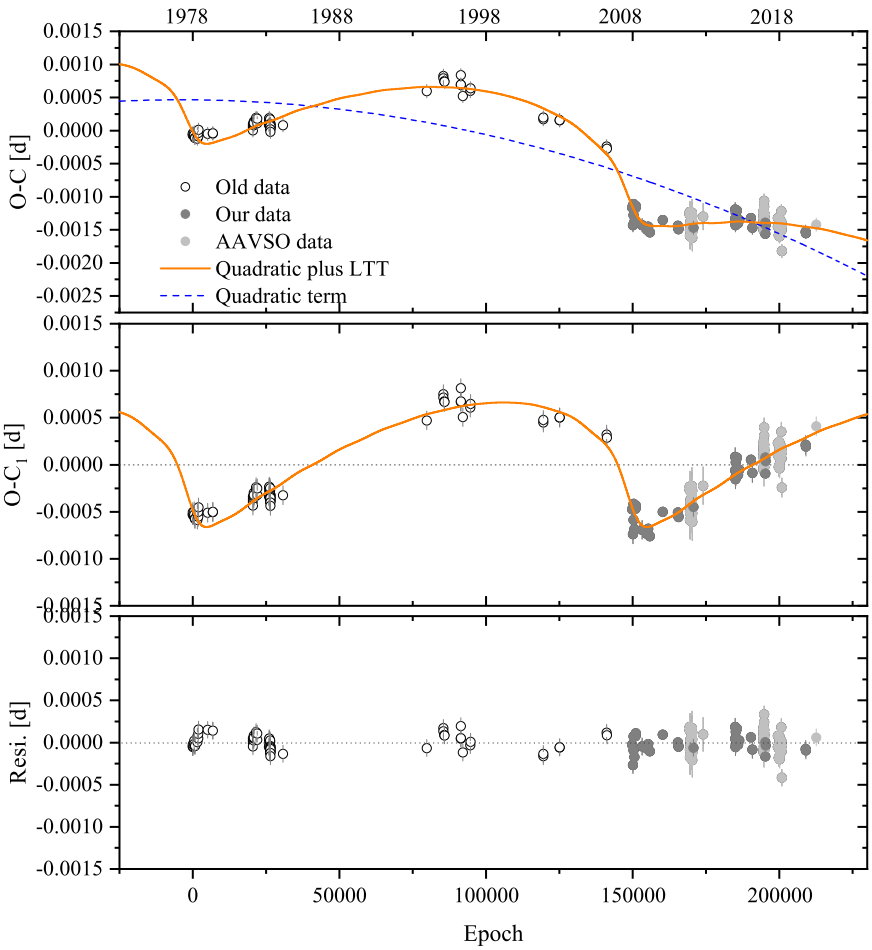

Figure 5. Latest $O-C$ diagram of HT Cas constructed with a quadratic plus LTT ephemeris. The black open circles denote all historical timings, while the dark gray solid circles refer to our eclipse timings and the light gray solid circles denote the AAVSO data. The orange solid line and blue dashed line in the top panel represent the best-fit model and the quadratic term of the model, respectively. The middle panel shows the LTTE orbit and the bottom panel displays the fit residuals from the full ephemeris.

Therefore, the change in rotational energy is

$$\Delta E_{\rm rot} \approx -7.36 \times 10^{33}\,{\rm J}. \quad (12)$$

The luminosity timescale is $\Delta E_{\rm rot}/L_2 = 718.6$ yr, much longer than the observed modulation cycle. This implies that even though less than 10% of the rotational energy is dissipated during the mechanism work, such a low stellar luminosity is unable to provide the required energy along a full oscillation cycle. This gives support to the interpretation of the apparent orbital period changes in terms of a light time effect. Similarly, it only means that the Applegate-like process is not the dominant mechanism here. Thus we suspect that the observed timing variations in HT Cas may result from a combination of a third-body perturbation and an Applegate and/or Applegate-like mechanism.

5. Conclusions

In this work, we have analyzed the orbital period variations of a short-period eclipsing CV, HT Cas. The results show that this system experiences a rapid orbital decay and a cyclic period oscillation. In general, the orbital period decrease in CVs arises from intrinsic AMLs by GR and/or MB. In particular, short-period systems are considered to be dominated by GR-driven AML. Our calculations, however, indicate that the observed decrease rate is an order of magnitude higher than the sum of both period decay rates caused by GR and MB, suggesting the presence of additional AML mechanisms. Recently, Schreiber et al. (2016) proposed the eCAML model to solve the white dwarf mass problem in CVs and found that it can not only explain the high average mass of CVs' white dwarfs but also solve other discrepancies between theory and observations. Using this model we found that the observed period decrease rate in HT Cas is basically consistent with the theoretically predicted value. We also explored the physical mechanism behind the eCAML model and found that the frictional AML following nova eruptions is the most promising candidate. Certainly, the actual evolution of HT Cas could be more complicated than the case we discussed above, and more observations and detailed tests are required in the near future.

Due to the fact that HT Cas has an extremely low-mass fully convective secondary star and needs a significant fraction of the available energy (>90%) to effect period changes, Applegate's mechanism struggles to explain the observed cyclic period fluctuation. Also, the alternative mechanism given by Lanza (2020) does not appear to be capable of explaining the orbital period oscillation in HT Cas. The most plausible explanation is the LTTE caused by the presence of an unseen circumbinary companion. The mass of the tertiary object was derived as $M_3 \sin i' = 0.013(\pm 0.002) M_\odot = 13.61(\pm 2.09) M_{\rm Jup}$. If this

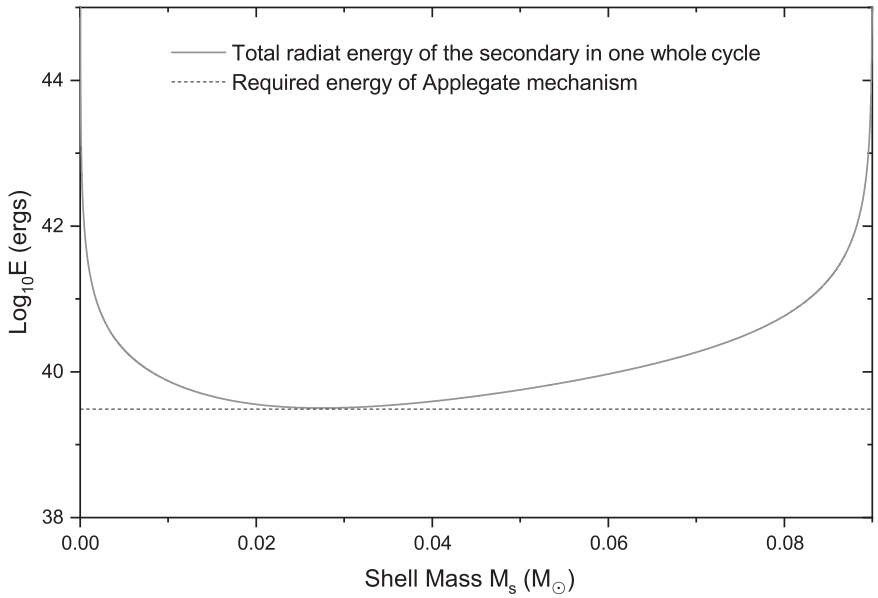

Figure 6. The gray solid line corresponds to the energy needed to generate the discovered period wiggle in HT Cas by applying Applegate's mechanism. M_s represents the supposed shell mass of the donor. The dashed horizontal line shows all radiant energy from the cool component in a full cycle of the $O - C$ modulation.

third body is coplanar to the orbital plane of the eclipsing pair (i.e., $i' = i = 81°$), its mass would match that of a giant planet on a very high eccentricity orbit ($e = 0.82$). Even though there have been multiple claims of planets around evolved star binaries, as yet, independent evidence for such planets is still quite lacking apart from the eclipse timing. Astrometry is expected to be an effective method to confirm the presence of these candidates (see Marsh 2018).

The present study reveals that HT Cas has significant extra AML due to the friction between the secondary star and the ejecta in a nova eruption and contains a high-eccentricity giant planet around it. This makes HT Cas one of the most peculiar short-period CVs, and continuous monitoring of eclipse timing in the system will provide an improved understanding of CV evolution. Moreover, HT Cas has been considered to be a modern counterpart of the ancient nova event in 722 CE (e.g., Duerbeck 1993; Hoffmann & Vogt 2020), potentially indicating that it could once have been a classical nova, although the nova shell around HT Cas is undetected by the Hα imaging method (Sahman et al. 2015). This provides indirect observational support for the frictional AML mechanism during nova eruptions. If all the results are reliable, how did the high-eccentricity giant planet form? Does the formation of a highly eccentric orbit have anything to do with the nova eruptions? These issues remain to be explored in future studies.

Acknowledgments

This work is partly supported by the National Natural Science Foundation of China (Nos. 11933008, 11922306), the Yunnan Fundamental Research Projects (Grant No. 2019FD083), West Light Foundation of the Chinese Academy of Sciences (No. E0290601), and the Foundation of Guizhou Educational Committee (No. Qianjiaohe KY Zi [2020]198). This work was also partially supported by the Open Project Program of the Key Laboratory of Optical Astronomy, National Astronomical Observatories, Chinese Academy of Sciences. The new photometric observations presented here were made with the Sino-Thai 70 cm and 2.4 m telescopes at the Yunnan Observatories and with the 85 cm and 2.16 m telescopes in Xinglong Observatory in China. We acknowledge the support of the staff of the Xinglong 2.16 m and 85 cm telescopes. We also thank observers from around the world for their contributions to the AAVSO data of HT Cas. IRAF is distributed by the National Optical Astronomy Observatories, which are operated by the Association of Universities for Research in Astronomy, Inc., under a cooperative agreement with the National Science Foundation.

ORCID iDs

Z.-T Han https://orcid.org/0000-0002-8412-7126
L.-Y. Zhu https://orcid.org/0000-0002-0796-7009

References

Ak, T., Ozkan, M. T., & Mattei, J. A. 2001, A&A, 369, 882
Almeida, L. A., & Jablonski, F. 2011, in IAU Symp. 276, The Astrophysics of Planetary Systems: Formation, Structure, and Dynamical Evolution (Cambridge: Cambridge Univ. Press), 495
Applegate, J. H. 1992, ApJ, 385, 621
Berriman, G., Kenyon, S., & Boyle, C. 1987, AJ, 94, 1291
Beuermann, K., Buhlmann, J., Diese, J., et al. 2011, A&A, 526, A53
Borges, B. W., Baptista, R., Papadimitriou, C., et al. 2008, A&A, 480, 481
Bours, M. C. P., Marsh, T. R., Parsons, S. G., et al. 2016, MNRAS, 460, 3873
Brinkworth, C. S., Marsh, T. R., Dhillon, V. S., et al. 2006, MNRAS, 365, 287
Bruch, A. 2000, A&A, 359, 998
Bruch, A. 2014, A&A, 566, A101
Delfosse, X., Forveille, T., Perrier, C., et al. 1998, A&A, 331, 581
Duerbeck, H. W. 1993, Cataclysmic Variables and Related Physics, 10 (Bristol: Institute of Physics Publishing), 77
Fang, X., Qian, S., Han, Z., et al. 2020, ApJ, 901, 113
Faulkner, J. 1971, ApJL, 170, L99
Feline, W. J., Dhillon, V. S., Marsh, T. R., et al. 2005, MNRAS, 364, 1158
Fleming, T. A., Schmitt, J. H. M. M., & Giampapa, M. S. 1995, ApJ, 450, 401
Garraffo, C., Drake, J. J., Alvarado-Gomez, J. D., et al. 2018, ApJ, 868, 60
Goździewski, K., Słowikowska, A., Dimitrov, D., et al. 2015, MNRAS, 448, 1118
Han, Z.-T., Qian, S.-B., Fernández Lajús, E., et al. 2015, NewA, 34, 1
Han, Z.-T., Qian, S.-B., Irina, V., et al. 2017, AJ, 153, 238
Hinse, T. C., Lee, J. W., Goździewski, K., et al. 2012, MNRAS, 420, 3609
Hodgkin, S. T., Jameson, R. F., & Steele, I. A. 1995, MNRAS, 274, 869
Hoffmann, S. M., & Vogt, N. 2020, MNRAS, 494, 5775
Hoffmeister, C. 1943, AN, 274, 36

Horne, K., Wood, J. H., & Stiening, R. F. 1991, ApJ, 378, 271
Horner, J., Marshall, J. P., Wittenmyer, R. A., et al. 2011, MNRAS Lett., 416, L11
Irwin, J. B. 1952, ApJ, 116, 211
Irwin, J. B. 1959, AJ, 64, 149
Johns-Krull, C. M., & Valenti, J. A. 1996, ApJL, 459, L95
Kato, T., Maehara, H., Miller, I., et al. 2012, PASJ, 64, 21
Khangale, Z. N., Potter, S. B., Kotze, E. J., et al. 2019, A&A, 621, A31
King, A. R., & Kolb, U. 1995, ApJ, 439, 330
Knigge, C., Baraffe, I., & Patterson, J. 2011, ApJS, 194, 28
Kraft, R. P., Mathews, J., & Greenstein, J. L. 1962, ApJ, 136, 312
Landau, L. D., & Lifshitz, E. M. 1975, Course of Theoretical Physics (Oxford: Pergamon)
Lanza, A. F. 2020, MNRAS, 491, 1820
Linsky, J. L., Wood, B. E., Brown, A., et al. 1995, ApJ, 455, 670
Liu, W.-M., & Li, X.-D. 2016, ApJ, 832, 80
Liu, W.-M., & Li, X.-D. 2019, ApJ, 870, 22
Marsh, T. R. 2018, Handbook of Exoplanets (Berlin: Springer), 96
Morin, J., Donati, J.-F., Forveille, T., et al. 2008, MNRAS, 384, 77
Mukai, K., Wood, J. H., Naylor, T., et al. 1997, ApJ, 475, 812
Nelemans, G., Siess, L., Repetto, S., et al. 2016, ApJ, 817, 69
Paczyński, B. 1967, AcA, 17, 287
Pala, A. F., Gänsicke, B. T., Belloni, D., et al. 2022, MNRAS, 510, 6110
Patterson, J. 1981, ApJS, 45, 517
Potter, S. B., Romero-Colmenero, E., Ramsay, G., et al. 2011, MNRAS, 416, 2202
Press, W. H., Teukolsky, S. A., Vetterling, W. T., & Flannery, B. P. 1992, Numerical recipes in FORTRAN. The art of scientific computing (2nd ed.; Cambridge: Cambridge Univ. Press)
Pringle, J. E. 1975, MNRAS, 170, 633
Qian, S. B., Han, Z. T., Fernández Lajús, E., et al. 2015, ApJS, 221, 17
Qian, S.-B., Liao, W.-P., Zhu, L.-Y., et al. 2010a, MNRAS Lett., 401, L34
Qian, S.-B., Liao, W.-P., Zhu, L.-Y., et al. 2010b, ApJL, 708, L66
Qian, S.-B., Liu, L., Liao, W.-P., et al. 2011, MNRAS Lett., 414, L16
Rappaport, S., Verbunt, F., & Joss, P. C. 1983, ApJ, 275, 713
Reiners, A., & Basri, G. 2007, ApJ, 656, 1121
Robertson, J. W., & Honeycutt, R. K. 1996, AJ, 112, 2248
Saar, S. H., & Linsky, J. L. 1985, ApJL, 299, L47
Sahman, D. I., Dhillon, V. S., Knigge, C., et al. 2015, MNRAS, 451, 2863
Schenker, K., Kolb, U., & Ritter, H. 1998, MNRAS, 297, 633
Schreiber, M. R., Zorotovic, M., & Wijnen, T. P. G. 2016, MNRAS Lett., 455, L16
Shao, Y., & Li, X.-D. 2012, ApJ, 745, 165
Sparks, W. M., & Sion, E. M. 2021, ApJ, 914, 5
Spruit, H. C., & Ritter, H. 1983, A&A, 124, 267
Taam, R. E., & Spruit, H. C. 2001, ApJ, 561, 329
Tody, D. 1986, Proc. SPIE, 627, 733
Tody, D. 1993, in ASP Conf. Ser. 52, Astronomical Data Analysis Software and Systems II, eds. R. J. Hanisch, R. J. V. Brissenden, & J. Barnes (San Francisco, CA: ASP), 173
van den Heuvel, E. P. J. 1994, Saas-Fee Advanced Course 22: Interacting Binaries (Berlin: Springer), 263
Vanbeveren, D. 1998, in The Brightest Binaries, ed. D. Vanbeveren, W. van Rensbergen, & C. De Loore (Boston: Kluwer Academic)
Verbunt, F., & Zwaan, C. 1981, A&A, 100, L7
Völschow, M., Schleicher, D. R. G., Banerjee, R., et al. 2018, A&A, 620, A42
Völschow, M., Schleicher, D. R. G., Perdelwitz, V., et al. 2016, A&A, 587, A34
Warner, B. 1995, Cataclysmic Variable Stars, Cambridge Astrophysics Series (Cambridge: Cambridge Univ. Press), 28
Webbink, R. F. 1985, Interacting Binary Stars (Cambridge: Cambridge Univ. Press), 39
Wenzel, W. 1987, AN, 308, 75
Wittenmyer, R. A., Horner, J., Marshall, J. P., et al. 2012, MNRAS, 419, 3258
Wood, J. H., Irwin, M. J., & Pringle, J. E. 1985, MNRAS, 214, 475
Wood, J. H., Naylor, T., Hassall, B. J. M., et al. 1995, MNRAS, 273, 772
Zhang, E.-H., Robinson, E. L., & Nather, R. E. 1986, ApJ, 305, 740